Journal of Asian Earth Sciences 151 (2018) 31–39

Contents lists available at ScienceDirect

Journal of Asian Earth Sciences

journal homepage: www.elsevier.com/locate/jseaes

Full length article

Rapid retreat of the East Asian summer monsoon in the middle Holocene and a millennial weak monsoon interval at 9 ka in northern China

Jinguo Dong[a,b,*], Chuan-Chou Shen[b,*], Xinggong Kong[c], Chung-Che Wu[b], Hsun-Ming Hu[b], Haojia Ren[d], Yi Wang[e]

[a] College of Geosciences, Nantong University, Nantong 226007, China
[b] High-Precision Mass Spectrometry and Environment Change Laboratory (HISPEC), Department of Geosciences, National Taiwan University, Taipei 106, Taiwan, ROC
[c] College of Geosciences, Nanjing Normal University, Nanjing 210097, China
[d] Department of Geosciences, National Taiwan University, Taipei 106, Taiwan, ROC
[e] Department of Geography, School of Global Studies, University of Sussex, Brighton BN1 9QJ, UK

ARTICLE INFO

Keywords:
Northern China
Stalagmite
East Asian summer monsoon
Holocene
Regional heterogeneous hydrological conditions

ABSTRACT

Knowledge of hydroclimatic dynamics in the East Asian monsoon region during the Holocene was hindered by few absolutely-dated and decadally-resolved proxy records in northern China. Here we present replicated carbonate $\delta^{18}O$ records of six stalagmites with sub-decadal to multi-decadal resolutions from the Lianhua cave to reveal a detailed evolution of the East Asian Summer Monsoon (EASM) intensity in northern China since 11.5 thousand years before present (ka BP, before 1950 CE). Our composite record shows that solar forcing dominated hydroclimatic changes regionally, including an intensified monsoon at the Holocene Optimum from the termination of Younger Dryas to 6.5 ka BP, and a subsequent multi-millennial weakening monsoon, that agrees with cave records in central and southern China. However, the EASM has retreated southwards more rapidly than the Indian summer monsoon after ~6.5 ka BP, resulting in aridity conditions occurring at 4.0 ka BP in northern China, which is almost 2000-year earlier than that in central and southern China. This north–south asynchroneity is likely related to the different regional responses among the coupling of the EASM, Indian summer monsoon, the solar forcing, and the differences in thermal forcing due to complex geographical configurations. In addition, a relative enrichment of 1‰ in ^{18}O data of the Lianhua record from 9.5 to 8.1 ka BP shows that the Holocene Optimum was punctuated by a millennial-long weakening monsoon interval, which is not registered among previous cave records in central and southern China. The fresh water-induced cold climate conditions in the North Atlantic region could create stronger East Asian winter monsoon, and induce a weakened EASM and a southward shift of rain belt in northern China. Therefore, it shall not be surprised that there are strong heterogeneities among regional hydroclimatic conditions across monsoonal China, given the complex interplay between external and internal forcing mechanisms over the entire Holocene.

1. Introduction

The Asian summer Monsoon (ASM), an essential part of the global climatic system, plays an important role in the global hydrological and energy cycles (Ding and Chan, 2005). Two subsystems of the ASM, East Asian summer monsoon (EASM) and Indian summer monsoon (ISM), not only interact with each other, but also are independent of each other, providing the majority of rainfall to the most densely populated areas of China (Wang et al., 2003). However, the ASM can vary significantly in different regions, simultaneously creating harmful periods of flood and drought across China. Unraveling the nature of the ASM variability and its forcing mechanisms is, therefore, essential both to understand the background of its present environment and hydroclimatic conditions, and to effectively predict future climate changes under the projected global warming scenarios (e.g., Huang et al., 2003; Ding and Chan, 2005; Wang et al., 2013).

Speleothems are as one kind of the most important natural archives mainly due to the advantages of absolute chronology (Wang et al., 2001, 2005, 2008; Yuan et al., 2004; Shen et al., 2012; Cheng et al., 2016). Previously published high-resolution stalagmite $\delta^{18}O$ sequences from southwestern China revealed that the ISM abruptly intensified after the end of Younger Dryas (YD), reached its maximum strength during the early-middle Holocene, and then decreased gradually over the past several thousand years (Wang et al., 2005; Dykoski et al.,

* Corresponding authors at: College of Geosciences, Nantong University, Nantong 226007, China.
E-mail addresses: dongjinguo1111@163.com (J. Dong), river@ntu.edu.tw (C.-C. Shen).

http://dx.doi.org/10.1016/j.jseaes.2017.10.016
Received 9 January 2017; Received in revised form 2 October 2017; Accepted 16 October 2017
Available online 16 October 2017
1367-9120/

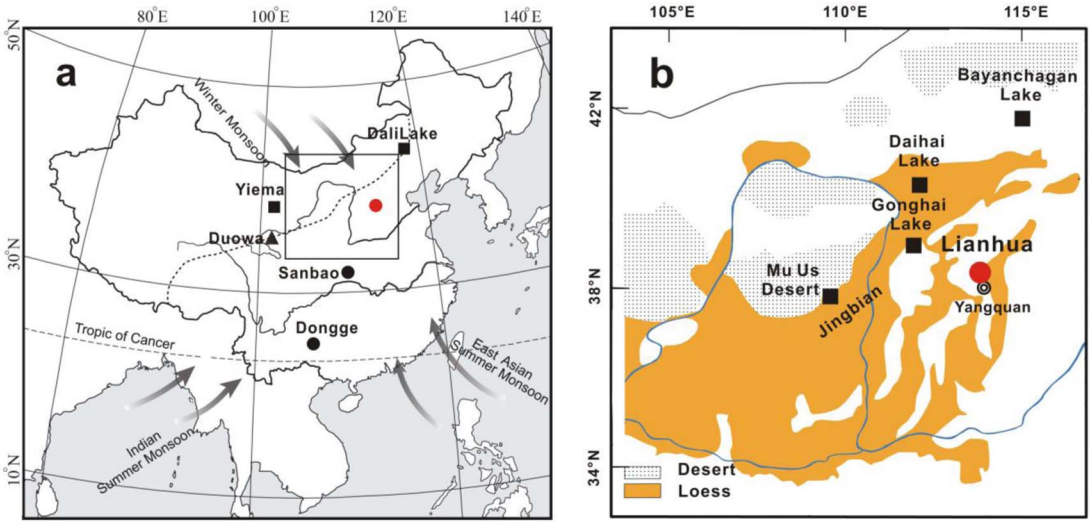

Fig. 1. (a) Location of Lianhua (this study, red circle), Sanbao (Wang et al., 2008; Dong et al., 2010) and Dongge (Wang et al., 2005) caves. Arrows show the modern monsoonal system in China, including the East Asian and Indian summer and winter monsoons. The summer monsoon is a steady flow of warm, moist air from the tropical oceans, and the winter monsoon is a flow of cold, dry air associated with the Siberian–Mongolian High. Dashed line denotes the averaged present-day limit of the summer monsoon. (b) An enlarged regional Chinese Loess Plateau map (32.9–43.7°N, 103.4–117.0°E). The locations of other records involving loess (triangle) and lake (squares) are also marked out in this map. (For interpretation of the references to colour in this figure legend, the reader is referred to the web version of this article.)

2005). This pattern closely follows the evolution of the Northern Hemisphere summer insolation (NHSI), and also agrees with earlier studies, indicating that the ISM intensity is closely related to the NHSI (Overpeck et al., 1996; Fleitmann et al., 2003; Gupta et al., 2003). Fleitmann et al. (2007) further inferred that the movement of the Intertropical Convergence Zone (ITCZ) induced by the changing NHSI might be the forcing mechanism driving the ISM variability.

On the other hand, the variability of the EASM during the Holocene as reconstructed from aeolian deposits (Lu et al., 2005; Li and Sun, 2006), peat and lacustrine sediments (Xiao et al., 2002, 2004; Jiang et al., 2006; Chen et al., 2015) in northern China showed different scenarios. For example, three sediment sequences respectively from Jinbian swamp (Xiao et al., 2002), Gonghai (Chen et al., 2015) and Daihai Lakes (Xiao et al., 2004), and two aeolian records from the Mu Us and Otindag dune fields (Lu et al., 2005) along the northernmost reach of present-day EASM (Fig. 1a) show that the monsoonal precipitation did not reach its maximum until ~8 thousand years ago (ka BP, before 1950 CE), and then began to decrease rapidly after ~4 ka BP. A lake-level sequence from Dali Lake in northern China yet reveals that the EASM precipitation reached the maximum during the early Holocene (11–6 ka BP) and then abruptly weakened after 6 ka BP (Goldsmith et al., 2017). Similar patterns were recorded by Bayanchagan and Yiema lakes in northern and northwestern China (Fig. 1, Jiang et al., 2006; Chen et al., 1999). At Duowa site in the western Loess Plateau, large sedimentation rates of the Holocene loess record suggest three discontinuous humid intervals: (1) from ~11.5 to 10 ka BP, (2) from ~8 to 6 ka BP, and (3) the wettest period from ~5 to 2.4 ka BP (Maher and Hu, 2006). Although Chinese stalagmite-inferred weakening monsoon events are coherent with the Holocene ice-rafting events [so-called Bond Events (Bond et al., 1997)] in the North Atlantic (Wang et al., 2005; Dykoski et al., 2005), regional hydrologic changes of the ASM may be, to some extent, heterogeneous across the monsoonal China (Chen J et al., 2015; Dong et al., 2015). Such contradictory views of the Holocene ASM changes raise the questions of: (1) what is the nature of the Holocene EASM variability in northern China? and (2) whether is there a spatial and temporal heterogeneity of hydrological-climatic conditions across the monsoonal China? To answer these questions, additional high-resolution, precisely-dated samples are needed, especially from northern China, where very limited absolutely-dated records are available so far.

Here we present a high-resolution, ^{230}Th-dated record of the EASM derived from six Holocene stalagmites from Lianhua Cave in northern China. We have added more ^{230}Th dates and new $\delta^{18}O$ samples to improve the accuracy and temporal resolution of the composite oxygen isotope records, although some data from three stalagmites have been reported recently (Dong et al., 2015). New records allow us to reconstruct a detailed EASM history with a unique focus on the latitudinal time-transgressive nature of the late-Holocene aridity at the end of the Holocene Optimum. We further discover the different regional responses of the ASM precipitation between 9.5 and 8.1 ka BP across the monsoonal China and identify the possible forcing mechanisms regulating regional hydrological changes therein.

2. Study site

Modern hydroclimate in northern China is strongly influenced by Asian monsoon and characterized by warm-wet summer and cool-dry winter. At the nearest meteorological station, Yangquan (Fig. 1b), the average monthly temperature (CE 1970–2000) shows a maximum of 24.0 °C in July and a minimum of −3.4 °C in January with the annual mean temperature of 11.2 °C (Fig. 2), and the annual mean precipitation is 515 mm and 73% of that falls between June and September during the EASM season.

Lianhua Cave (38°10′N, 113°43′E), at an elevation 1200 m, is located in the west flank of Taihang Mountain, semi-arid Shanxi Province, in northern China (Fig. 1). The cave, with a narrow entrance of 0.5 m in

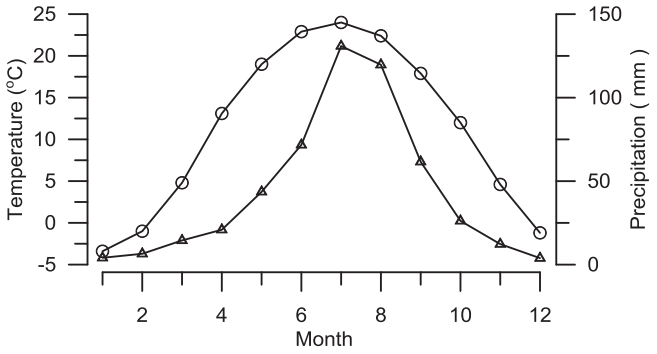

Fig. 2. Average monthly air temperature (circle) and precipitation (triangle) in the Yangquan station during 1970–2000 CE.

Table 1
Uranium and thorium isotopic compositions and ^{230}Th ages for stalagmites LH1, LH4, LH5, LH6, LH9 and LH30 by MC-ICP-MS.

ID/Depth (mm)	^{238}U ppb	^{232}Th ppt	δ^{234}U measured[a]	^{230}Th/^{238}U activity[c]	Age (ka BP) uncorrected	Age (ka BP) corrected[c,d]	δ^{234}U initial[b]
***LH1-11**	195.50 ± 0.32	658.2 ± 6.9	2761.8 ± 7.7	0.01085 ± 0.00019	0.25 ± 0.0056	0.23 ± 0.010	2764.1 ± 7.6
***LH1-93**	247.73 ± 0.34	1155.2 ± 5.4	4987.1 ± 7.8	0.03286 ± 0.00035	0.54 ± 0.0064	0.52 ± 0.010	4995.3 ± 7.8
***LH1-134**	263.51 ± 0.35	630.1 ± 7.3	5405.0 ± 9.7	0.05049 ± 0.00026	0.80 ± 0.0046	0.79 ± 0.0067	5418.0 ± 9.7
***LH1-148**	291.83 ± 0.58	462.2 ± 4.6	6041.8 ± 27	0.08455 ± 0.00059	1.25 ± 0.010	1.25 ± 0.010	6064.2 ± 8.7
***LH1-186**	159.20 ± 0.22	12515.5 ± 74.1	5231.1 ± 8.2	0.1248 ± 0.0020	3.33 ± 0.055	2.82 ± 0.26	3089.9 ± 7.1
LH4-10	100.38 ± 0.15	2030.4 ± 8.7	1660.3 ± 4.7	0.1471 ± 0.0015	6.12 ± 0.063	5.92 ± 0.12	1688.6 ± 4.8
LH4-38	134.58 ± 0.35	3697.8 ± 15.8	1660.0 ± 7.6	0.1589 ± 0.0019	6.63 ± 0.084	6.36 ± 0.16	1690.4 ± 7.7
LH4-53	130.61 ± 0.47	2362.4 ± 11.4	1714.0 ± 14.0	0.1706 ± 0.0015	6.98 ± 0.073	6.81 ± 0.11	1747.6 ± 14.2
LH4-93	164.81 ± 0.44	1648.2 ± 7.2	1717.2 ± 7.5	0.1741 ± 0.0015	7.12 ± 0.066	7.03 ± 0.082	1752.0 ± 7.7
LH4-138	259.62 ± 0.86	2847.9 ± 12.7	1713.9 ± 11.1	0.1979 ± 0.0013	8.15 ± 0.067	8.04 ± 0.085	1753.6 ± 11
LH4-145	263.03 ± 1.7	2936.9 ± 12.2	1768.5 ± 19.8	0.2034 ± 0.0018	8.21 ± 0.096	8.11 ± 0.11	1809.8 ± 20
LH4-156	283.52 ± 0.63	627.7 ± 6.0	1726.0 ± 7.5	0.2052 ± 0.0010	8.42 ± 0.050	8.40 ± 0.051	1767.7 ± 7.6
LH4-166	329.10 ± 0.71	1955.6 ± 8.1	1713.1 ± 6.9	0.2123 ± 0.0013	8.77 ± 0.060	8.71 ± 0.067	1756.1 ± 7.1
LH4-181	328.42 ± 0.26	7345.4 ± 29.0	1699.9 ± 3.0	0.2254 ± 0.0017	9.38 ± 0.072	9.16 ± 0.13	1744.8 ± 3.1
LH4-213	360.54 ± 0.98	1022.6 ± 8.2	1637.3 ± 8.9	0.2313 ± 0.00089	9.87 ± 0.053	9.84 ± 0.054	1683.8 ± 9.2
LH5-14	143.26 ± 0.70	2043.5 ± 8.1	1713.0 ± 12	0.08771 ± 0.00076	3.51 ± 0.035	3.37 ± 0.077	1730.1 ± 12
***LH5-31**	154.31 ± 0.16	2457.9 ± 5.8	1792.7 ± 2.7	0.0932 ± 0.00077	3.62 ± 0.031	3.47 ± 0.081	1810.7 ± 2.8
LH5-54	139.51 ± 0.51	883.6 ± 5.8	1771.4 ± 8.7	0.09667 ± 0.00066	3.80 ± 0.029	3.74 ± 0.032	1790.5 ± 8.8
LH5-62	121.36 ± 0.43	8363.0 ± 33	1689.3 ± 8.3	0.1376 ± 0.0020	5.65 ± 0.085	4.97 ± 0.348	1713.5 ± 8.6
***LH5-100**	117.75 ± 0.11	1200.2 ± 4.3	1676.2 ± 2.1	0.1394 ± 0.00085	5.74 ± 0.037	5.64 ± 0.062	1703.4 ± 2.2
LH5-148	111.05 ± 0.30	2058.0 ± 7.9	1655.0 ± 7.2	0.1662 ± 0.0013	6.95 ± 0.058	6.77 ± 0.11	1687.3 ± 7.4
LH5-161	353.88 ± 1.0	656.6 ± 5.9	1676.4 ± 8.5	0.2084 ± 0.00078	8.72 ± 0.044	8.71 ± 0.045	1718.4 ± 8.7
LH5-181	313.12 ± 0.31	3580.0 ± 11	1683.5 ± 3.1	0.2262 ± 0.0013	9.47 ± 0.056	9.36 ± 0.079	1728.9 ± 3.1
***LH5-224**	360.87 ± 0.44	2374.8 ± 5.5	1650.4 ± 3.0	0.2314 ± 0.0010	9.80 ± 0.044	9.74 ± 0.055	1696.7 ± 3.1
LH5-230	408.45 ± 0.41	459.0 ± 27	1680.7 ± 3.1	0.23891 ± 0.00059	10.04 ± 0.029	10.03 ± 0.029	1729.3 ± 3.2
***LH5-300**	559.09 ± 0.67	1967.3 ± 5.9	1595.9 ± 2.8	0.2434 ± 0.00076	10.63 ± 0.037	10.59 ± 0.041	1643.3 ± 2.9
LH5-377	734.52 ± 1.8	451.4 ± 5.7	1565.9 ± 7.5	0.2633 ± 0.00081	11.64 ± 0.052	11.63 ± 0.052	1618.4 ± 7.7
***LH6-5**	137.61 ± 0.39	5347.1 ± 18.6	2854.3 ± 10.4	0.1153 ± 0.0013	3.24 ± 0.040	2.98 ± 0.14	2878.9 ± 10.6
***LH6-48**	136.76 ± 0.65	4396.7 ± 14.8	2696.9 ± 15.5	0.1277 ± 0.0014	3.76 ± 0.046	3.53 ± 0.12	2723.4 ± 15.7
LH9-7	143.22 ± 0.23	570.5 ± 9.3	2705.3 ± 7.4	0.0517 ± 0.00040	1.47 ± 0.012	1.44 ± 0.019	2716.9 ± 7.4
LH9-28	124.79 ± 0.18	381.5 ± 3.5	2084.7 ± 5.1	0.05816 ± 0.00038	2.01 ± 0.014	1.99 ± 0.019	2096.5 ± 5.2
LH9-58	99.00 ± 4.8	3210.2 ± 8.8	4249.3 ± 287	0.1555 ± 0.0079	3.21 ± 0.25	3.05 ± 0.25	4286.7 ± 289
LH9-102	115.68 ± 0.15	3209.6 ± 12	3148.0 ± 6.4	0.1650 ± 0.0021	4.35 ± 0.056	4.18 ± 0.10	3185.9 ± 6.6
***LH30-14**	162.53 ± 0.22	6406.0 ± 25	3321.8 ± 5.5	0.1122 ± 0.0019	2.80 ± 0.049	2.56 ± 0.13	3346.5 ± 5.6
***LH30-14**	165.38 ± 0.24	4459.7 ± 13	3365.0 ± 6.6	0.1092 ± 0.0013	2.69 ± 0.032	2.53 ± 0.088	3389.7 ± 6.7
***LH30-38**	155.45 ± 0.24	27670.8 ± 101	3040.1 ± 6.1	0.1617 ± 0.0038	4.37 ± 0.11	3.21 ± 0.59	3068.3 ± 8.0
***LH30-44**	159.63 ± 0.17	3304.9 ± 7.9	4112.0 ± 4.7	0.1338 ± 0.0011	2.82 ± 0.024	2.71 ± 0.058	4144.4 ± 4.7
***LH30-59**	164.36 ± 0.18	3639.9 ± 9.1	3160.3 ± 3.7	0.1213 ± 0.0012	3.15 ± 0.033	3.01 ± 0.077	3187.9 ± 3.8
***LH30-63**	143.77 ± 0.29	11342.5 ± 29	3849.5 ± 9.9	0.1657 ± 0.0027	3.71 ± 0.063	3.28 ± 0.22	3886.0 ± 10
***LH30-72**	170.01 ± 0.25	11414.6 ± 36.5	4521.1 ± 9.1	0.2345 ± 0.0028	4.66 ± 0.059	4.34 ± 0.17	4577.6 ± 9.5
***LH30-122**	144.99 ± 0.28	19040.6 ± 71	3191.8 ± 9.0	0.2211 ± 0.0035	5.81 ± 0.096	4.98 ± 0.43	3237.5 ± 9.9
***LH30-122**	140.99 ± 0.49	12034.9 ± 50	2404.9 ± 12	0.1939 ± 0.0025	5.46 ± 0.073	4.89 ± 0.30	2945.8 ± 12

The bold values with a star (*) symbol are the new ^{230}Th ages in this study.
Analytical errors are 2σ of the mean.

[a] $\delta^{234}U = ([^{234}U/^{238}U]_{activity} - 1) \times 1000$.

[b] δ^{234}U corrected was calculated based on ^{230}Th age (T), i.e., $\delta^{234}U_{initial} = \delta^{234}U_{measured} \times e^{\lambda_{234} * T}$, T is corrected age.

[c] $[^{230}Th/^{238}U]_{activity} = 1 - e^{-\lambda_{230} T} + (\delta^{234}U_{measured}/1000)[\lambda_{230}/(\lambda_{230} - \lambda_{234})](1 - e^{-(\lambda_{230} - \lambda_{234}) T})$, where T is the age. Decay constants are 9.1577×10^{-6} yr^{-1} for ^{230}Th, 2.8263×10^{-6} yr^{-1} for ^{234}U and 1.55125×10^{-6}yr^{-1} for ^{238}U (Cheng et al., 2000).

[d] Age (before 1950 CE) corrections were made using a ^{230}Th/^{232}Th atomic ratio of 4 ± 2 ppm, which is value for material at secular equilibrium with the crustal ^{232}Th/^{238}U value of 3.8 and arbitrarily assumed uncertainty of 50%.

diameter and 250-m long passage, is overlain by 50-m Ordovician limestone of the Ma-Jia-Gou Group (Qian, 1960). A 20-m wide, 15-m high chamber, is located at the end of the cave and abundant with a variety of fossil speleothems, including stalagmites, stalactites and flowstones. Relative humidity in the deepest chamber is 98–100%. A cave temperature of 11 °C matches ambient annual mean ground temperature. The densely-forested vegetation above the cave consists primarily of temperate deciduous broadleaf trees.

3. Samples and methods

Six calcite stalagmites were collected from Lianhua cave (Table 1), among which three (LH4, LH5 and LH9) have been reported previously by Dong et al. (2015). Each stalagmite was sectioned along its growth axis. A new stalagmite, LH30, with an obvious hiatus at 65 mm from the top, is 125-mm in length. There is an absence of observable hiatus for new stalagmites of LH1 and LH6, 190 mm and 65 mm in length, respectively.

Sixteen subsamples of the three newly-collected stalagmites (LH1, LH6, and LH30), 100–200 mg each, were drilled for U-Th chemistry (Shen et al., 2003) and ^{230}Th dating (Shen et al., 2002, 2012). Uranium-thorium isotopic measurements were performed on a multi-collection inductively coupled plasma mass spectrometer (MC-ICP-MS), Thermo Finnigan NEPTUNE, in the High-precision Mass Spectrometry and Environment Change Laboratory (HISPEC), Department of Geosciences, National Taiwan University (Shen et al., 2012). A gravimetrically calibrated (Cheng et al., 2013) triple-spike, ^{229}Th-^{233}U-^{236}U, isotope dilution method was employed to correct mass bias and determine U-Th contents and isotopic compositions (Shen et al., 2012). Half-lives of U-Th nuclides used for ^{230}Th age calculation are given in Cheng et al. (2013). Uncertainties in the U-Th isotopic data and ^{230}Th dates, relative to 1950 CE, are given at the two-sigma (2σ) level or two standard deviations of the mean ($2\sigma_m$) unless otherwise noted.

For stable isotopic measurements, 342 subsamples, 10–20 μg each, were drilled with a 0.3 mm-diameter carbide dental burr at 1-mm intervals. The correspondent temporal resolution is 4–55 years. The

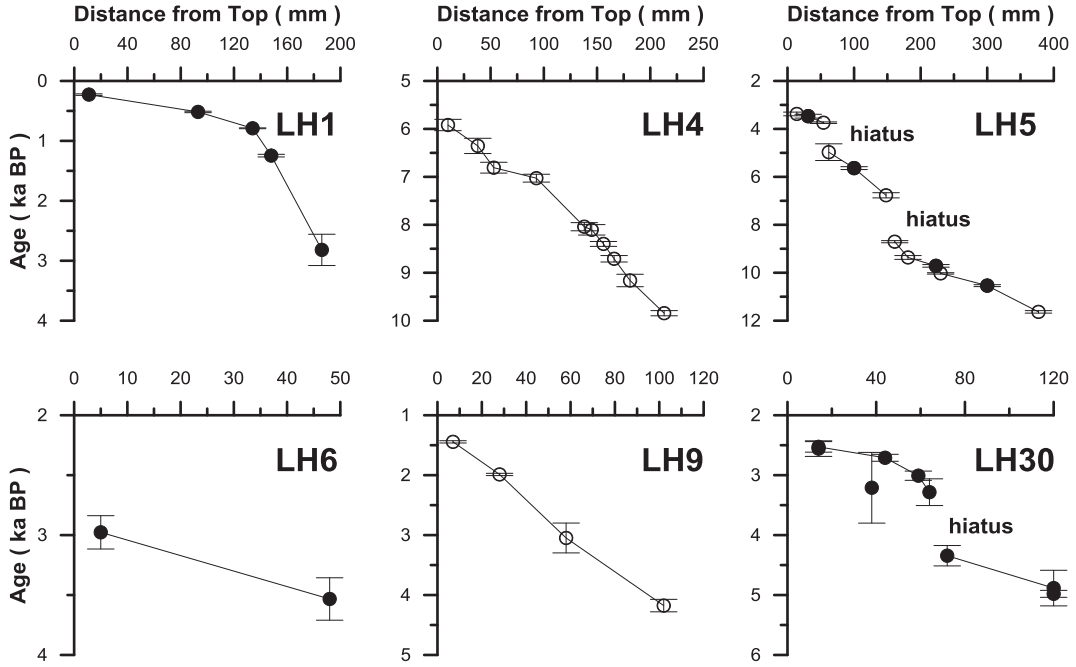

Fig. 3. Plot of the age models for six Lianhua stalagmites: LH1, LH4, LH5, LH6, LH9 and LH30. Black filled circles are new ^{230}Th data in this study.

analysis was conducted on a Finnigan-MAT 253 mass spectrometer equipped with an automatic Kiel Carbonate Device at the College of Geography Science, Nanjing Normal University. Results are reported relative to the Vienna Pee Dee Belemnite (VPDB) and standardization was accomplished using NBS-19. Precision of $\delta^{18}O$ values is ± 0.06‰ at the 1-sigma level. A statistical regression approach RAMPFIT (Mudelsee, 2000), a weighted least-square method that determines a ramp between states of a certain record, was employed to Lianhua cave $\delta^{18}O$ records to estimate the timing, duration and transition of monsoonal events.

4. Results

4.1. Chronology

Uranium-thorium isotopic compositions and ^{230}Th dates of all stalagmites are listed in Table 1. Linear interpolation between ^{230}Th dates, in a stratigraphic order, was used to develop the age models. Age-depth plots are given in Fig. 3. The chronological results show that stalagmite LH1 deposited from 2.8 to 0.2 ka BP, LH6 from 3.6 to 2.9 ka BP, and LH30 from 5.0 to 2.4 ka BP with a hiatus between 4.3 and 3.3 ka BP. The calculated growth rates are 24–283 μm/year for LH1, 43 μm/year for LH6, and 18–88 μm/year for LH30, respectively.

4.2. Oxygen isotope records

The sound evaluation of Lianhua cave $\delta^{18}O$ records, using Hendy Test (Hendy, 1971) and Replication Test (Dorale and Liu, 2009) by Dong et al. (2015), has demonstrated that stalagmites deposited under oxygen isotopic equilibrium conditions and had insignificant kinetic fractionation. The $\delta^{18}O$ records of our five stalagmites, for example, match each other over the contemporaneous growth periods within the dating error (Fig. 4). The only exception is the LH30 $\delta^{18}O$ record, which is 0.6‰ more depleted in ^{18}O than other records (Fig. 4). Systematic differences between coeval stalagmite $\delta^{18}O$ records within the same cave were reported before, such as in Hulu (Wang et al., 2001), Dongge (He et al., 2005) and Huangye (Tan et al., 2011) caves in China. Fairchild et al. (2006) suggested that these offsets should be attributable to prior calcite precipitation in different water flow paths. By a shift of −0.6‰, a good overlapping between LH30 and our other records (Fig. 4) supports previous arguments of that the stalagmite $\delta^{18}O$ records can still preserve the original hydroclimatic signals (e.g., Wang et al., 2001; Yuan et al., 2004; Tan et al., 2011; Dong et al., 2015).

Early studies from southern China showed that changes in Chinese cave stalagmite $\delta^{18}O$ mainly recorded variations in summer monsoon intensity on decadal to orbital scales (e.g., Wang et al., 2001, 2005; Yuan et al., 2004; Cheng et al., 2009a). However, some traditional paleo-moisture (or precipitation) proxies and model simulations suggested that Chinese cave stalagmite $\delta^{18}O$ should more likely reflect changes in moisture sources and/or water vapor pathways, and it may not be considered as a reliable indicator of the strength of the ASM (Maher, 2008; LeGrande and Schmidt, 2009; Pausata et al., 2011; Liu et al., 2015, 2017). Recently, Cheng et al. (2016) extended the early ideas presented in the original studies (Wang et al., 2001; Yuan et al., 2004) and further clarified that the stalagmite $\delta^{18}O$-inferred ASM variations reflect a mean state of summer monsoon intensity or integrated moisture transport rather than the amount of local precipitation. In other words, a higher proportion of regional ASM rainfall and/or higher spatially integrated monsoon rainfall between the tropical monsoon sources and the cave site would result in more negative local stalagmite $\delta^{18}O$. This interpretation is supported by a modeling study (Liu et al., 2014) and an empirical study (Orland et al., 2015), which suggested that local stalagmite records represent proxies of EASM intensity in northern China. More importantly, at Dali Lake, located ~600 km north of Lianhua Cave, a lake-level record regarded traditionally as a typical proxy of the EASM intensity, is highly correlated with Lianhua Cave $\delta^{18}O$ records on precessional and millennial timescales (r^2 = 0.8, see Fig. 3 of Goldsmith et al., 2017). Higher Dali lake levels correspond to depleted cave deposits isotopic compositions, and vice versa. On the basis of theoretical, empirical and model studies, we interpret Lianhua Cave stalagmite $\delta^{18}O$ records as qualitative proxies for regional precipitation and intensity of the EASM (at least in northern China), with lower values expressing a stronger EASM, and vice versa.

Our spliced stalagmite $\delta^{18}O$ records range from −7.2‰ to −11.3‰ (Fig. 4). The $\delta^{18}O$ values abruptly decreased by 3.3‰ during the transition from YD to the initiation of the Holocene at 11.5 ka BP, and lingered with the most negative averaged value of −10.2‰ at an interval from 11.5 to 6.5 ka BP, punctuated by a relatively positive

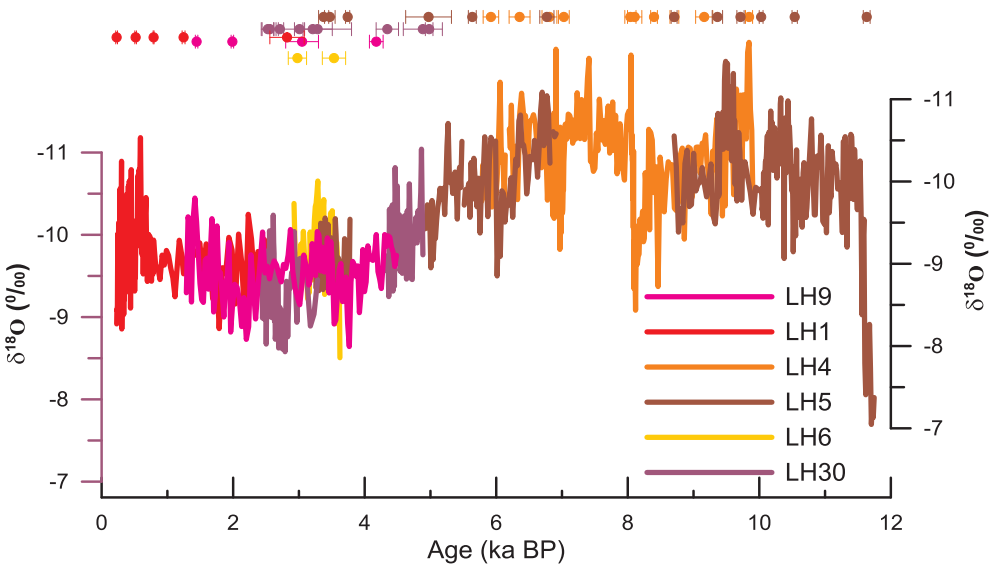

Fig. 4. The composed $\delta^{18}O$ time series of six stalagmites from Lianhua Cave. Samples LH4, LH5 and LH9 have been reported by Dong et al. (2015). ^{230}Th ages with 2σ uncertainty are color-coded by stalagmite.

millennial-scale $\delta^{18}O$ interval from 9.5 to 8.1 ka BP. There was a millennial-scale increasing trend from 6.5 to 4.0 ka BP. After 4.0 ka BP, $\delta^{18}O$ values hovered between −8.5‰ to −11.0‰ until 0.2 ka BP.

5. Discussions

5.1. Regional monsoon changes on millennial-orbital scales

A comparison of the composed Lianhua record to precisely dated contemporaneous speleothem records of Sanbao Cave from central China and Dongge Cave from southern China (Fig. 1a) is given in Fig. 5. The recovery of the YD at 11.5 ± 0.05 ka BP in Lianhua record matches ones in Sanbao and Dongge time series within dating error. Different regional monsoons generally reached their maximum intensities at the early-middle Holocene, followed by a gradual weakening trend until late Holocene (Fig. 5, Table 2). This consistence supports that insolation is the primary driver controlling the entire ASM hydroclimate (e.g., Cheng et al., 2016). The maximum of summer insolation

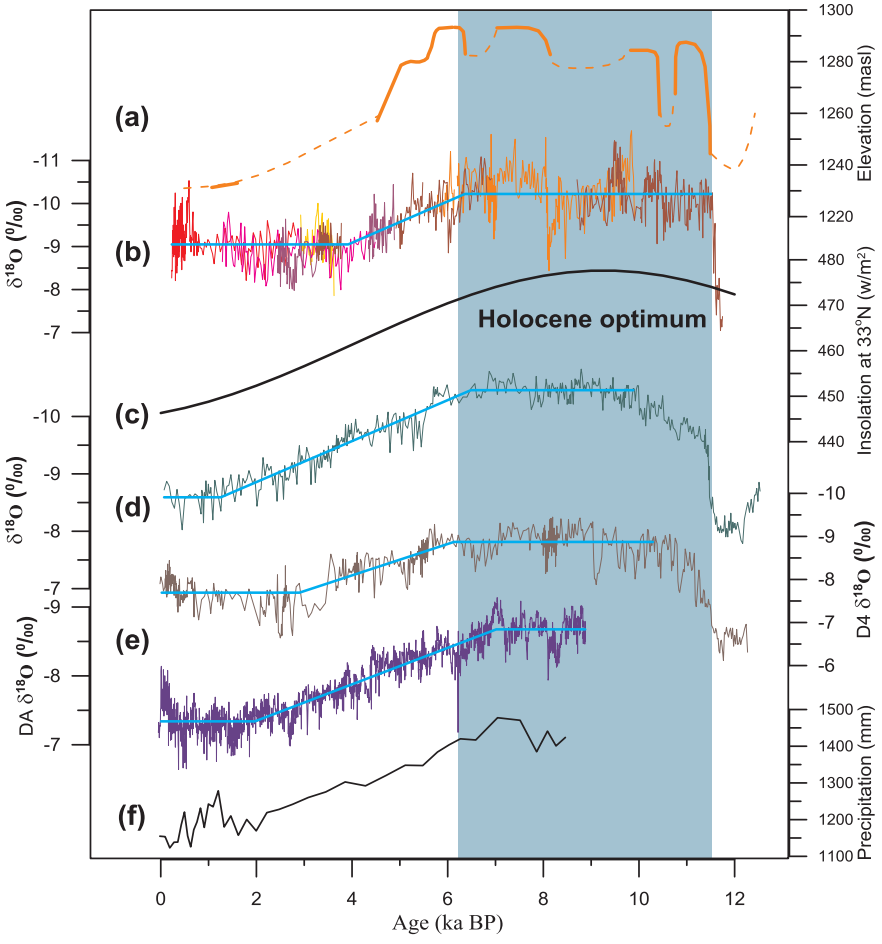

Fig. 5. A comparison of the stalagmite $\delta^{18}O$ time series, lake-level record and annual precipitation sequence along a latitudinal transect. (a) Lake level record of Lake Dali, northern China (Goldsmith et al., 2017). The $\delta^{18}O$ records from caves of (b) Lianhua (38°10′N, 113°43′E), northern China, (d) Sanbao (31°4′N, 110°26′E; Dong et al., 2010), central China, and (e) Dongge [25°17′N, 108°5′E; two stalagmites: AD (deep blue) and D4 (dark brown), Wang et al., 2005; Dykoski et al., 2005], southwestern China. (c) Black line denotes mid-July solar insolation at 33°N (Berger, 1978), and (f) Pollen-based annual precipitation reconstructed from Lake Xingyun, Yunnan Plateau, southwestern China (Chen et al., 2014). Light-gray bar denotes the Holocene Optimum, well related with the strong EASM interval between 11.6 and 6.5 ka BP. Heavy cyan lines illustrate the long-term trends as defined by RAMPFIT (Mudelsee, 2000) for the timing of the onset of the late-Holocene aridity across the monsoonal China.(For interpretation of the references to colour in this figure legend, the reader is referred to the web version of this article.)

Table 2
Parameters used for RAMPFIT analysis and the onset time of the late-Holocene drought.[a]

Cave (sample)	Onset time of the late-Holocene drought (a BP)	Ending time of the Holocene Optimum (a BP)	n	t (1)	t (n)	STD fit	*t*1–*t*2 search (a BP)
Lianhua cave	3920 ± 190	6360 ± 90	670	230	11510	0.709	230–5220/5550–11510
Sanbao cave	1350 ± 60	6490 ± 60	359	70	9981	0.701	70–5749/2567–9981
Dongge cave – (DA)	1970 ± 60	7020 ± 60	2115	5	8876	0.569	5–4409/4409–8876
Dongge cave –(D4)	2900 ± 110	6130 ± 50	666	20	10290	0.607	20–4050/4050–10290

[a] *n*: Number of data point, *t* (1): start of interval, *t* (*n*): end of interval, STD fit: standard deviation of data, *t*1 − *t*2 search: intervals from which *t*1/*t*2 were chosen.

occurred at around 9 ka BP in the Northern Hemisphere (Kutzbach and Gallimore, 1986) could significantly strengthen the thermal contrast between Asian landmass and the low-latitude tropical Ocean, therefore result in an intensified ASM in China from early to middle Holocene.

Although there is a general agreement on orbital timescales for an increasing trend of speleothem $\delta^{18}O$ after ~6.5 ka BP, there is also a striking asynchroneity about the way stalagmite $\delta^{18}O$ values increased among different cave records. A statistical regression approach, namely RAMPFIT (Mudelsee, 2000), was used to objectively determine the onset timing of the late-Holocene drought for each cave record across the China. The dataset and results are listed in Table 2, and the statistically calculated RAMPs are plotted in Fig. 5. The combined Lianhua record indicates that the EASM rapidly retreated southwards between 6.5 and 4.0 ka BP, resulting in a serious late-Holocene aridity occurring in the studying region after 4.0 ka BP (Fig. 5b). This drought interval is also well documented in other proxies and/or archives on/around the Loess Plateau in northern China. For example, a well-dated closed-basin lake level record in northeastern China spanning the period from 0 to 16 ka BP indicates the EASM minimum occurred during the late-Holocene from 4.0 ka BP to the present (Fig. 5a). This is generally consistent with the increased probability of eolian-land activity from 3.2 ka BP to the present based on 89 optically stimulated luminescence (OSL) dates of eolian sand samples collected from four major sandlands located along the modern monsoon border in northern China (Wang et al., 2014). Our results are also in broad agreement with many pollen records from the Chinese Loess Plateau area that demonstrate the occurrence of relatively dry conditions from 4 ka BP to the present (Xiao et al., 2004; Zhao et al., 2009). By contrast, the ASM over central and southwestern China gradually retreated from 7.0 to 2.0 ka BP (Fig. 5d, e), characterized by a gradual increase of $\delta^{18}O$ values as recorded in Sanbao and Dongge Caves. At Xingyun Lake of Yunnan Province dominantly controlled by the ISM, the quantitative pollen-based annual precipitation reconstruction exhibits a clear decreasing trend from 7.2 to 2.0 ka BP, and subsequently maintains the minimum level until the present (Fig. 5f, Chen et al., 2014). Similar results were also found in the ISM influenced regions (Fleitmann et al., 2003; Gupta et al., 2003; Hong et al., 2003). Accordingly, we suggest that the late-Holocene aridity occurred most likely at 4.0 ka BP in northern China, while it might begin later at 2.0 ka BP in the central and southern China (Fig. 5).

The spatial heterogeneity of summer rainfall across monsoonal China is well known with modern observations, often described colloquially as “flood in the south and drought in the north”, or “drought in the south and flood in the north” (Hu and Feng, 2001). Summer precipitation could have a “− + −“ or “+ − +” spatial pattern in southern, central, and northern sectors of China (Ding et al., 2008). Our findings also support the idea about the north-south asynchronous changes of the ASM at the end of the Holocene Humid Period across China (Zhao et al., 2013; Zhang et al., 2017). The observed latitudinal heterogeneity of hydroclimate conditions across monsoonal China over the recent decades and in the Holocene suggests that the ASM variability should be more complicated than previously thought.

This asynchronism could be related to the different regional responses to the coupling among the EASM, ISM, and the NHSI forcing, and also the differences in thermal forcing due to complex geographical configuration (Wang et al., 2003; Cai et al., 2010). As a subtropical monsoon system, the EASM is not only influenced by tropical monsoon trough closely linked to the insolation-forced ITCZ, but also regulated by the northwestern Pacific subtropical high (NPSH), a subsiding branch of the Hadley Circulation in the tropics. Recent modeling results and fresh geological records (Lézine et al., 2017) indicated that the timing of the southward retreat of the ITCZ at the end of Holocene Humid Period occurred in two steps in Asian monsoonal region. These two steps are respectively dated at 5.0 and 2.7 ka BP. At 5.0 ka BP, the orbitally-driven retreat of the tropic ITCZ induced a southward displacement of the NPSH, where the EASM rain belt is co-located at the northwestern boundary (Wang et al., 2003, 2013; Huang et al., 2003; Tan, 2016). Meanwhile, the sea surface temperature (SST) gradient between the west and east tropical Pacific Ocean as compiled in Koutavas and Joanides (2012) suggests that an E1Niño-like condition should have prevailed during the late Holocene (Tan, 2016). A rapidly decreasing of the SST gradient between 5.5 and 4.0 ka BP (Fig. 6 of Koutavas and Joanides (2012)) could result in weaker Walker and Hadley circulation and a southward shift of the NPSH, which could move the associated rain belt southward into central and southern China, and later into the tropical western Pacific warm pool. The whole process rapidly weakened the EASM precipitation in northern China (Huang et al., 2003; Wang et al., 2013; Chen et al., 2015), corresponding to increased $\delta^{18}O$ values in our Lianhua cave records. On the other hand, changes in the Pacific thermal condition cannot modulate the intensity of the ISM because it gradually decreases in response to orbitally-driven southward shift of the ITCZ from 7.0 ka BP (Fleitmann et al., 2003, 2007; Chen et al., 2014). After 2.7 ka BP, a further southward retreat of the ITCZ could displace the ASM front out of the mainland China, resulting in complete arid conditions across the whole monsoonal China (Lézine et al., 2017).

5.2. A millennial-scale weakening monsoonal intensity at 9 ka BP in northern China

The Holocene Optimum in East Asian territory, as proposed by An et al. (2000), was considered as a peak in precipitation or moisture in monsoonal China during the Holocene. For example, the prevailing summer monsoon is revealed in stalagmite records (Fig. 5d, e) of Sanbao Cave in central China, and Dongge Cave in southern China (Fig. 1). However, a long-time anomalous climatic reversal is clearly recorded by the Lianhua $\delta^{18}O$ records, which are characterized by the ^{18}O enrichment of ~1‰ between 9.5 and 8.1 ka BP (Fig. 6b). Near Gonghai Lake, located 50 km northwest of the Lianhua Cave (Fig. 1), the concentration of broadleaf trees has obviously declined, which inferred the regional annual precipitation decreased by ~80 mm from 9.5 to 8.5 ka BP (Fig. 6d, Chen et al., 2015). Further north from our cave, a proxy from Dali Lake (Fig. 6a, Goldsmith et al., 2017) also suggests that the lake-level obviously has declined by ~10 m, possibly associated with a relatively weakened summer monsoon at this interval. Within our dating uncertainties, three independent proxies (Fig. 6a, b, d) all show a reduction in monsoon intensity during this interval, implying that this weakening is of large-scale in the space, rather than a localized event in the arid and semi-arid region of northern China.

Another striking feature of this weakening event is its asymmetrical

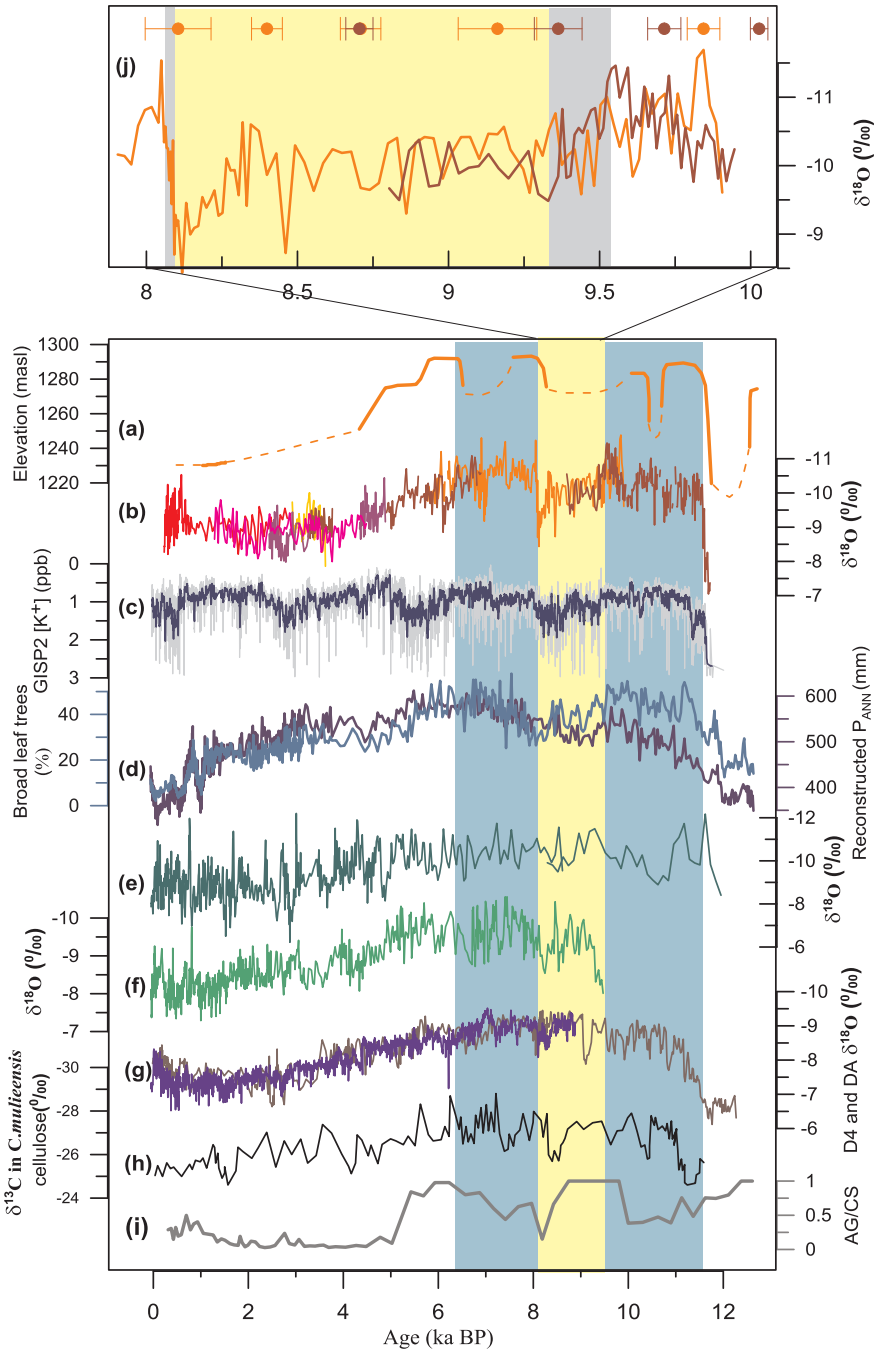

Fig. 6. A comparison of proxy records from northern to southern China. (a) Lake level record of Lake Dali, northern China (Goldsmith et al., 2017), (b) Lianhua stalagmites $\delta^{18}O$ (this study). (c) Nine-dot smoothed GISP2 potassium ion proxy for the Siberian High (Mayewski et al., 1997). (d) Percentage of broad-leaf tree and its pollen-inferred annual precipitation in Gonghai Lake, northern China (Chen et al., 2015). Stalagmites $\delta^{18}O$ records from (e) Jiuxian (Cai et al., 2010) and (f) Heshang (Hu et al., 2008) caves, respectively, in central China. (g) $\delta^{18}O$ records of two Dongge stalagmites, DA and D4, from southwestern China, where the summer monsoon precipitation are mainly influenced by ISM (Wang et al., 2005; Dykoski et al., 2005). (h) Proxy record for the ISM from $\delta^{13}C$ time series of the *C. mulieensis* remains cellulose in the Hongyuan peat bog in the eastern Tibetan Plateau (Hong et al., 2003). (i) The ratio of AC/CS (*A. granulate/C. stelligera*), from the Huguangyan Maar Lake, Guangdong province, regarded as an indicator of the EAWM with high/low values of the ratio indicating strong/weak EAWM (Wang L et al., 2008, 2012). Light-blue bar denotes a stalagmite-inferred strong early-Holocene EASM interval between 11.6 and 6.5 ka BP, which is slightly interrupted by a weakening event between 9.5 and 8.0 ka BP (yellow bar). (j) Lianhua stalagmites $\delta^{18}O$ (this study) records with an age interval of 8–10 ka BP. Gray bars in the enlarged figure show the abrupt end and gradual onset of the long-term weakened monsoon event. Ages and 2σ errors are color-coded by records. (For interpretation of the references to colour in this figure legend, the reader is referred to the web version of this article.)

temporal structure, showing a gradual initiation (~200 yrs) at 9.5 ka BP, and an abrupt recovery (< 50 yrs) at 8.1 ka BP (Fig. 6j). During this 1400-yr interval, regional hydroclimatic conditions obviously deteriorated, and attained the culmination at the 8.2 ka BP. This distinct asymmetrical temporal structure is also clearly observed during the period of the YD event. The full transition into the YD, for example, took 380-yr according the layer-counted Qiantian cave record (Liu et al., 2008, and references therein), and the transition out of the YD only took about 20-yr according to Kulishu cave record (Ma et al., 2012 and references therein). Moreover, the duration of the YD is ~1290-yr, very close to ~1400-yr of our interval. Such a good similarity between two weakening monsoon events may indicate the asymmetrical climatic features of the last glacial period could extend into the early Holocene because they are likely to share the same driving forces under similar glacial boundary conditions (Cheng et al., 2009b).

Similar to the initialization of the YD, this weakening EASM event may be triggered also by a massive influx of fresh water into the North Atlantic region (Barber et al., 1999; McManus et al., 2004; Chen et al., 2015), resulting in a slowdown of the Atlantic meridional overturning circulation, a rapid cooling of the North Atlantic, a southward shift of the ITCZ as well as a weakening of the EASM (Mayewski et al., 1997; Guo et al., 2000; Wang et al., 2005; Chen et al., 2015). An induced synchronous millennial-long drought occurred over the entire Asian summer monsoon region from 9.5 to 8.0 ka BP (Fig. 6, Guo et al., 2000; Chen et al., 2015). However, different regions apparently experienced different arid conditions (Wang et al., 2012; Chen J et al., 2015). The reducing trend in stalagmite $\delta^{18}O$ enrichment from north to south China (Figs. 5 and 6b, e–g), in addition to previously published paleohydrological records from northern and southern China (Fig. 6a, d and h), suggest that droughts in northern China should be severer than

in other regions, and that the severity should be relieved moving southward between 9.5 and 8.0 ka BP.

As previously reviewed by Mayewski et al. (2004), the widespread, cold-dry climate interruption from 9.0 to 8.0 ka BP is unique among the Holocene rapid climate change (RCC) intervals, and it occurred at a time when larger Northern Hemispheric ice sheets were still present. The prominent enrichment as shown in the Lianhua $\delta^{18}O$ record is very sensitive to the North Hemispheric high-latitude forcing (Dong et al., 2015; and references therein) because it is much closer to the northwestern boundary of the ASM. The cold climatic conditions in the Northern Atlantic region would have promoted stronger Siberian High (Fig. 6c, Mayewski et al., 1997), resulting in strong East Asian winter monsoon (EAWM) occurred at 10.0–8.0 ka BP, as recorded in Huguangyan Maar Lake, Guandong, southern China (Fig. 6i, Wang L et al., 2008, 2012). However, during the early Holocene, the strengthening of the millennial-scale EAWM was unlikely to be as strong as during the glacial period, and would not have displaced the ASM front out of the Chinese mainland especially as the summer insolation was high in the Northern Hemispheric resulting in a strong ASM during the early Holocene (Fig. 5). We speculate that the relatively strong EAWM event can induce a weakened EASM, and a southward shift of rainfall-belt in northern China, resulting in lower precipitation in northern China than in southern China (Fig. 6, yellow shade).

6. Conclusions

We composed an absolutely-dated and high-resolution speleothem $\delta^{18}O$ record for the entire Holocene in northern China. Our Lianhua records shows that the orbital forcing has dominated controls of hydroclimate changes, including a stronger EASM at the Holocene Optimum from 11.5 to 6.5 ka BP, and a subsequent multi-millennial weakening EASM, that broadly agrees with stalagmite records in central and southern China. However, a detailed comparison of our record to precisely-dated contemporaneous stalagmite records from other caves shows that: (1) the aridity was more severe in northern China than in southern China between 9.5 and 8.1 ka BP, which may be contributed to an intensified EAWM event during this interval; and (2) the late-Holocene aridity in northern China occurred at around 4 ka BP, almost 2000-year earlier than that in central and southern China. This latitudinal time-transgressive nature of the late-Holocene aridity could be attributed to the stepwise southward retreat of the ASM following the orbitally-driven ITCZ shifts with obvious two jumps. Moreover, the variation of the SST gradient in the tropical Pacific may exert an important impact on the EASM precipitation changes because it affects the NPSH, which regulates monsoonal front migration.

Acknowledgements

We thank Dr. Xiuyang Jiang, Jilong Li and Wei Zhang for their help with field work and isotope analyses. Thanks are also given to two anonymous reviewers for his/her critical and instructive comments. This research was supported by grants from the National Nature Science Foundation of China (No. 41472317, 41102216), Jiangsu Overseas Research and Training Program for University Prominent Young and Middle-aged Teachers and Presidents, and the research opportunities fund of University of Sussex. Funding was also provided by grants from Taiwan ROC MOST (104-2119-M-002-003, 105-2119-M-002-001, 105-2811-M-002-094) and the National Taiwan University (105R7625).

References

An, Z.S., Porter, S.C., Kutzbach, J.E., Wu, X.H., Wang, S.M., Liu, X.D., Li, X.Q., Zhou, W.J., 2000. Asychronous Holocene optimum of the East Asian monsoon. Quatern. Sci. Rev. 19, 743–762.

Barber, D.C., Dyke, A., Hillaire-Marcel, C., Jennings, A.E., Andrews, J.T., Kerwin, M.W., Bilodeau, G., McNeely, R., Southon, J., Morehead, M.D., Gagnon, J.M., 1999. Forcing of the cold event of 8200 years ago by catastrophic drainage of Laurentide lakes. Nature 400, 344–348.

Berger, A.L., 1978. Long-term variations of caloric insolation resulting from the Earth's orbital elements. Quatern. Res. 9, 139–167.

Bond, G., Showers, W., Cheseby, M., Lotti, R., Almasi, P., deMenocal, P., Priore, P., Cullen, H., Hajdas, I., Bonani, G., 1997. A pervasive millennial-scale cycle in North Atlantic. Science 278, 1257–1266.

Cai, Y.J., Tan, L.C., Cheng, H., An, Z.S., Edwards, R.L., Kelly, M.J., Kong, X.G., Wang, X.F., 2010. The variation of summer monsoon precipitation in central China since the last deglaciation. Earth Planet. Sci. Lett. 291, 21–31.

Chen, F.H., Chen, X.M., Chen, J.H., Zhou, A.F., Wu, D., Tang, L.Y., Zhang, X.J., Huang, X.Z., Yu, J.Q., 2014. Holocene vegetation history, precipitation change and Indian summer monsoon evolution documented by Xingyun Lake, Southwest China. J. Quat. Sci. 29, 661–674.

Chen, F.H., Shi, Q., Wang, J.M., 1999. Environmental changes documented by sedimentation of Lake Yiema in arid China since the Late Glaciation. J. Paleolimnol. 22, 159–169.

Chen, F.H., Xu, Q.H., Chen, J.H., Birks, H.J., Liu, J.B., Zhang, S.R., Jin, L.Y., An, C.B., Telford, R.J., Cao, X.Y., Wang, Z.L., Zhang, X.J., Selvaraj, K., Lu, H.Y., Li, Y.C., Zheng, Z., Wang, H.P., Zhou, A.F., Dong, G.H., Zhang, J.W., Huang, X.Z., Bloemendal, J., Rao, Z.G., 2015a. East Asian summer monsoon precipitation variability since the last deglaciation. Sci. Report 5, 11186.

Chen, J.H., Chen, F.H., Feng, S., Huang, W., Liu, J.B., Zhou, A.F., 2015b. Hydroclimatic changes in China and surroundings during the Medieval Climate Anomaly and Little Ice Age: Spatial patterns and possible mechanisms. Quatern. Sci. Rev. 107, 98–111.

Cheng, H., Edwards, R.L., Broecker, W.S., Denton, G.H., Kong, X.G., Wang, Y.J., Zhang, R., Wang, X.F., 2009a. Ice age terminations. Science 326, 248–252.

Cheng, H., Edwards, R.L., Hoff, J., Gallup, C.D., Richards, D.A., Asmerom, Y., 2000. The half-lives of uranium-234 and thorium-230. Chem. Geol. 169, 17–33.

Cheng, H., Edwards, R.L., Shen, C.-C., Polyak, V.J., Asmerom, Y., Woodhead, J., Hellstrom, J., Wang, Y.J., Kong, X.G., Spötl, C., Wang, X.F., Alexander, E.C., 2013. Improvements in ^{230}Th dating, ^{230}Th and ^{234}U half-life values, and U-Th isotopic measurements by multi-collector inductively coupled plasma mass spectrometry. Earth Planet. Sci. Lett. 372, 82–91.

Cheng, H., Edwards, R.L., Sinha, A., Spötl, C., Yi, L., Chen, S.T., Kelly, M., Kathayat, G., Wang, X.F., Li, X.L., Kong, X.G., Wang, Y.J., Ning, Y.F., Zhang, H.W., 2016. The Asian monsoons over the past 640,000 years and ice age terminations. Nature 534, 640–647.

Cheng, H., Fleitmann, D., Edwards, R.L., Wang, X.F., Cruz, F.W., Auler, A.S., Mangini, A., Wang, Y.J., Kong, X.G., Burns, S.J., Matter, A., 2009b. Timing and structure of the 8.2 kyr B.P. event inferred from $\delta^{18}O$ records of stalagmites from China, Oman and Brazil. Geology 37 (11), 1007–1010.

Ding, Y.H., Chan, C.L., 2005. The East Asian summer monsoon: An overview. Meteorol. Atmos. Phys. 89, 117–142.

Ding, Y.H., Wang, Z.Y., Sun, Y., 2008. Inter-decadal variation of the summer precipitation in East China and its association with decreasing Asian summer monsoon. Part I: observed evidences. Int. J. Climatol. 28, 1139–1161.

Dong, J.G., Shen, C.C., Kong, X.G., Jiang, X.Y., 2015. Reconciliation of hydroclimate sequences from Loess Plateau and low-latitude zones in the East Asian monsoon territory over the past 14,500 years. Palaeogeogr. Palaeoclimatol. Palaeoecol. 435, 127–135.

Dong, J.G., Wang, Y.J., Cheng, H., Hardt, B., Edwards, R.L., Kong, X.G., Wu, J.Y., Chen, S.T., Liu, D.B., Jiang, X.Y., Zhao, K., 2010. A high-resolution stalagmite record of the Holocene East Asian monsoon from Mt Shennongjia, central China. The Holocene 20, 257–264.

Dorale, J., Liu, Z.H., 2009. Limitations of Hendy Test criteria in judging the paleoclimatic suitability of speleothems and the need for replication. J. Cave Karst Stud. 71, 73–80.

Dykoski, C.A., Edwards, R.L., Cheng, H., Yuan, D.X., Cai, Y.J., Zhang, M.L., Lin, Y.S., Qing, J.M., An, Z.S., Revenaugh, J., 2005. A high-resolution, absolute-dated Holocene and deglacial Asian monsoon record from Dongge Cave, China. Earth Planet. Sci. Lett. 233, 71–86.

Fairchild, I.J., Smith, C.L., Baker, A., Fuller, L., Spötl, C., Mattey, D., McDermott, F.E.I.M.F., 2006. Modification and preservation of environmental signals in speleothems. Earth Sci. Rev. 75, 105–153.

Fleitmann, D., Burns, S.J., Mangini, A., Mudelsee, M., Kramers, J., Villa, I., Neff, U., Al-Subbary, A.A., Buettner, A., Hippler, D., Matter, A., 2007. Holocene ITCZ and Indian monsoon dynamics recorded in stalagmites from Oman and Yemen (Socotra). Quatern. Sci. Rev. 26, 170–188.

Fleitmann, D., Burns, S.J., Mudelsee, M., Neff, U., Kramers, J., Mangini, A., Matter, A., 2003. Holocene forcing of the Indian monsoon recorded in a stalagmite from Southern Oman. Science 300, 1737–1739.

Goldsmith, Y., Broecker, W.S., Xu, H., Polissar, P.J., deMenocal, P.B., Porat, N., Lan, J.H., Cheng, P., Zhou, W.J., An, Z.S., 2017. Northward extent of East Asian monsoon covaries with intensity on orbital and millennial timescales. Proc. Natl. Acad. Sci. U.S.A. 114, 1817–1821.

Guo, Z.T., Petit-Maire, N., Kröpelin, S., 2000. Holocene non-orbital climatic events in present-day arid areas of northern Africa and China. Global Planet. Change 26, 97–103.

Gupta, A.K., Anderson, D.M., Overpeck, J.T., 2003. Abrupt changes in the Asian southwest monsoon during the Holocene and their links to the North Atlantic Ocean. Nature 421, 354–356.

He, Y.Q., Wang, Y.J., Kong, X.G., Cheng, H., 2005. High resolution stalagmite $\delta^{18}O$ records over the past 1000 years from Dongge Cave in Guizhou. Chin. Sci. Bull. 50, 1003–1008.

Hendy, C.H., 1971. The isotopic geochemistry of speleothems-I. The calculation of the effects of different modes of formation on the isotopic composition of speleothems and their applicability as palaeoclimatic indicators. Geochim. Cosmochim. Acta 35,

801–824.
Hong, Y.T., Hong, B., Lin, Q.H., Zhu, Y.X., Shibata, Y., Hirota, M., Uchida, M., Leng, X.T., Jiang, H.B., Xu, H., Wang, H., Yi, L., 2003. Correlation between Indian ocean monsoon and north Atlantic climate during the Holocene. Earth Planet. Sci. Lett 211, 371–380.
Hu, C.Y., Henderson, G.M., Huang, J.H., Xie, S.C., Sun, Y., Johnson, K.R., 2008. Quantification of Holocene Asian monsoon rainfall from spatially separated cave records. Earth Planet. Sci. Lett. 266, 221–232.
Hu, Q., Feng, S., 2001. A southward migration of centennial-scale variations of drought/flood in Eastern China and the western United States. J. Clim. 14, 1323–1328.
Huang, R.H., Wen, C., Ding, Y.H., Li, C.Y., 2003. Studies on the monsoon dynamics and the interaction between monsoon and ENSO cycle. Chin. J. Atmos. Sci. 27, 484–502 (in Chinese).
Jiang, W.Y., Guo, Z.T., Sun, X.J., Wu, H.B., Chu, G.Q., Yuan, B.Y., Hatté, C., Guiot, J., 2006. Reconstruction of climate and vegetation changes of Lake Bayanchagan (Inner Mongolia): Holocene variability of the East Asian monsoon. Quatern. Res. 65, 411–420.
Koutavas, A., Joanides, S., 2012. El Niño-southern oscillation extrema in the Holocene and Last Glacial Maximum. Paleoceanography 27, 1–2.
Kutzbach, J.E., Gallimore, R.G., 1986. The influence of changing orbital parameters and surface boundary conditions on climate simulation for the past 18,000 years. J. Atmos. Sci. 43, 1726–1759.
LeGrande, A.N., Schmidt, G.A., 2009. Sources of Holocene variability of oxygen isotopes in paleoclimate archives. Clim. Past 5, 441–455.
Lézine, A.-M., Ivory, S.J., Braconnot, P., Marti, O., 2017. Timing of the southward retreat of the ITCZ at the end of the Holocene Humid Period in Southern Arabia: Data-model comparison. Quatern. Sci. Rev. 164, 68–76.
Li, S.H., Sun, J.M., 2006. Optical dating of Holocene dune sands from the Hulun Buir Desert, northeastern China. Holocene 16, 457–462.
Liu, D.B., Wang, Y.J., Cheng, H., Edwards, R.L., Kong, X.G., Wang, X.F., Wu, J.Y., Chen, S.T., 2008. A detailed comparison of Asian monsoon intensity and Greenland temperature during the Allerød and Younger Dryas events. Earth Planet. Sci. Lett. 272, 691–697.
Liu, J.B., Chen, J.H., Zhang, X.J., Li, Y., Rao, Z.G., Chen, F.H., 2015. Holocene East Asian summer monsoon records in northern China and their inconsistency with Chinese stalagmite $\delta^{18}O$ records. Earth Sci. Rev. 148, 194–208.
Liu, J.B., Chen, S.Q., Chen, J.H., Zhang, Z.P., Chen, F.H., 2017. Chinese cave $\delta^{18}O$ records do not represent northern East Asian summer monsoon rainfall. Proc. Natl. Acad. Sci. U.S.A. 114, E2987–E2988.
Liu, Z.Y., Wen, X.Y., Brady, E.C., Otto-Bliesner, B., Yu, G., Lu, H.Y., Cheng, H., Wang, Y.J., Zheng, W.P., Ding, Y.H., Edwards, R.L., Cheng, J., Liu, W., Yang, H., 2014. Chinese cave records and the East Asia Summer Monsoon. Quatern. Sci. Rev. 83, 115–128.
Lu, H.Y., Miao, X.D., Zhou, Y.L., Mason, J., Swinehart, J., Zhang, J.F., Zhou, L.P., Yi, S.W., 2005. Late Quaternary aeolian activity in the Mu Us and Otindag dune fields (north China) and lagged response to insolation forcing. Geophys. Res. Lett. 32, L21716.
Ma, Z.B., Cheng, H., Tan, M., Edwards, R.L., Li, H.C., You, C.F., Duan, W.H., Wang, X., Kelly, M.J., 2012. Timing and structure of the Younger Dryas event in northern China. Quatern. Sci. Rev. 41, 83–93.
Maher, B.A., 2008. Holocene variability of the East Asian summer monsoon from Chinese cave records: a re-assessment. Holocene 18, 861–866.
Maher, B.A., Hu, M.Y., 2006. A high-resolution record of Holocene rainfall variations from the western Chinese Loess Plateau: antiphase behaviour of the African/Indian and East Asian summer monsoons. Holocene 16, 309–319.
Mayewski, P.A., Meeker, L.D., Twickler, M.S., Whitlow, S., Yang, Q.Z., Lyons, W.B., Prentice, M., 1997. Major features and forcing of high-latitude northern hemisphere atmospheric circulation using a 110,000-year-long glaciochemical series. J. Geophys. Res.-Oceans 102, 26345–26366.
Mayewski, P.A., Rohling, E.E., Stager, J.C., Karlén, W., Maasch, K.A., Meeker, L.D., Meyerson, E.A., Gasse, F., Kreveld, S., Holmgren, K., Lee-Thorp, J., Rosqvist, G., Rack, F., Staubwasser, M., Schneider, R.R., Steig, E.J., 2004. Holocene climate variability. Quatern. Res. 62, 243–255.
McManus, J.F., Francois, R., Gherardi, J.-M., Keigwin, L.D., Brown-Leger, S., 2004. Collapse and rapid resumption of Atlantic meridional circulation linked to deglacial climate changes. Nature 428, 834–837.
Mudelsee, M., 2000. Ramp function regression: A tool for quantifying climate transitions. Comput. Geosci. 2000 (26), 293–307.
Orland, I.J., Edwards, R.L., Cheng, H., Kozdon, R., Mellissa, C., Valley, J.W., 2015. Direct measurements of deglacial monsoon strength in a Chinese stalagmite. Geology 43, 555–558.
Overpeck, J., Anderson, D., Trumbore, S., Prell, W., 1996. The southwest Indian Monsoon over the past 18,000 years. Clim. Dyn. 12 (3), 213–225.
Pausata, F., Battisti, D., Nisancioglu, K., Bitz, C., 2011. Chinese stalagmite $\delta^{18}O$ controlled by changes in the Indian monsoon during a simulated Heinrich event. Nat. Geosci. 4, 474–480.
Qian, X.P., 1960. Development of the Carbonate Karst, Shanxi plateau. Hydrogeol. Eng. Geol. 4 (3), 19–23 (in Chinese).
Shen, C.-C., Cheng, H., Edwards, R.L., Moran, S.B., Edmonds, H.N., Hoff, J.A., Thomas, R.B., 2003. Measurement of attogram quantities of ^{231}Pa in dissolved and particulate fractions of seawater by isotope dilution thermal ionization mass spectroscopy. Anal. Chem. 75, 1075–1079.
Shen, C.-C., Edwards, R.L., Cheng, H., Dorale, J.A., Thomas, R.B., Bradley Moran, S., Weinstein, S.E., Edmonds, H.N., 2002. Uranium and thorium isotopic and concentration measurements by magnetic sector inductively coupled plasma mass spectrometry. Chem. Geol. 185, 165–178.
Shen, C.-C., Wu, C.-C., Cheng, H., Edwards, R.L., Hsieh, Y.-T., Gallet, S., Chang, C.-C., Li, T.-Y., Lam, D.D., Kano, A., Hori, M., Spotl, C., 2012. High-precision and high-resolution carbonate ^{230}Th dating by MC-ICP-MS with SEM protocols. Geochim. Cosmochim. Acta 99, 71–86.
Tan, M., 2016. Circulation background of climate patterns in the past millennium: Uncertainty analysis and re-reconstruction of ENSO-like state. Sci. China Earth Sci. 59, 1225–1241.
Tan, L.C., Cai, Y.J., An, Z.S., Edward, R.L., Cheng, H., Shen, C.C., Zhang, H.W., 2011. Centennial- to decadal-scale monsoon precipitation variability in the semi-humid region, northern China during the last 1860 years: Records from stalagmites in Huangye Cave. The Holocene 21, 287–296.
Wang, Y.J., Cheng, H., Edwards, R.L., An, Z.S., Wu, J.Y., Shen, C.-C., Dorale, J.A., 2001. A high-resolution absolute-dated Late Pleistocene monsoon record from Hulu Cave, China. Science 294, 2345–2348.
Wang, B., Clemens, S.C., Liu, P., 2003. Contrasting the Indian and East Asian monsoons: implications on geologic timescales. Mar. Geol. 201, 5–21.
Wang, Y.J., Cheng, H., Edwards, R.L., He, Y.Q., Kong, X.G., An, Z.S., Wu, J.Y., Kelly, M.J., Dykoski, C.A., Li, X., 2005. The Holocene Asian monsoon: links to solar changes and North Atlantic Climate. Science 308, 854–857.
Wang, L., Lu, H.Y., Liu, J.Q., Gu, Z.Y., Mingram, J., Chu, G.Q., Li, J.J., Rioual, P., Negendank, J.F.W., Han, J.T., Liu, T.S., 2008a. Diatom-based inference of variations in the strength of Asian winter monsoon winds between 17,500 and 6000 calendar years BP. J. Geophys. Res.-Atmos. 113, D21101.
Wang, Y.J., Cheng, H., Edwards, R.L., Kong, X.G., Shao, X.H., Chen, S.T., Wu, J.Y., Jiang, X.Y., Wang, X.F., An, Z.S., 2008b. Millennial- and orbital-scale changes in the East Asian monsoon over the past 224,000 years. Nature 451, 1090–1093.
Wang, L., Li, J.J., Lu, H.Y., Gu, Z.Y., Rioual, P., Hao, Q.Z., Mackay, A.W., Jiang, W.Y., Cai, B.G., Xu, B., Han, J.T., Chu, G.Q., 2012. The East Asian winter monsoon over the last 15,000 years: its links to high-latitudes and tropical climate systems and complex correlation to the summer monsoon. Quatern. Sci. Rev. 32, 131–142.
Wang, B., Xiang, B., Lee, J.Y., 2013. Subtropical high predictability establishes a promising way for monsoon and tropical storm predictions. Proc. Natl. Acad. Sci. USA 110, 2718–2722.
Wang, H., Chen, J., Zhang, X., Chen, F., 2014. Palaeosol development in the Chinese Loess Plateau as an indicator of the strength of the East Asian summer monsoon: evidence for a mid-Holocene maximum. Quatern. Int. 334, 155–164.
Xiao, J.L., Nakamura, T., Lu, H.Y., Zhang, G.Y., 2002. Holocene climate changes over the desert/loess transition of north-central China. Earth Planet. Sci. Lett. 197, 11–18.
Xiao, J.L., Xu, Q.H., Nakamura, T., Yang, X.L., Liang, W.D., Inouchi, Y., 2004. Holocene vegetation variation in the Daihai Lake region of north-central China: a direct indication of the Asian monsoon climatic history. Quatern. Sci. Rev. 23, 1669–1679.
Yuan, D., Cheng, H., Edwards, R.L., Dykoski, C.A., Kelly, M.J., Zhang, M.L., Qing, J.M., Lin, Y.S., Wang, Y.J., Wu, J.Y., Dorale, J.A., An, Z.S., Cai, Y.J., 2004. Timing, duration, and transitions of the last interglacial Asian monsoon. Science 304, 575–578.
Zhang, E.L., Zhao, C., Xue, B., Liu, Z.G., Yu, Z.C., Chen, R., Shen, J., 2017. Millennial-scale hydroclimate variations in southwest China linked to tropical Indian Ocean since the last glacial maximum. Geology 45, 435–438.
Zhao, C., Chang, Y.-P., Chen, M.-T., Liu, Z.G., 2013. Possible reverse trend in Asian summer monsoon strength during the late Holocene. J. Asian Earth Sci. 69, 102–112.
Zhao, Y., Yu, Z., Chen, F., Zhang, J., Yang, B., 2009. Vegetation response to Holocene climate change in monsoon-influenced region of China. Earth Sci. Rev. 97, 242–256.